Plant Soil (2014) 377:407–422
DOI 10.1007/s11104-013-2003-7

REGULAR ARTICLE

Mechanisms of trichome-specific Mn accumulation and toxicity in the Ni hyperaccumulator *Alyssum murale*

David H. McNear Jr. · Joseph V. Kupper

Received: 23 July 2013 / Accepted: 6 December 2013 / Published online: 17 January 2014
© Springer Science+Business Media Dordrecht 2014

Abstract
Background and aims Mechanisms of Mn accumulation and toxicity in and around trichomes on the Ni hyperaccumulator *Alyssum murale* were investigated.
Methods Plants were grown aeroponically with variable amounts of Mn and Ni. Total metals were determined and electron microprobe analysis (EMPA) and synchrotron-based micro x-ray fluorescence (μ-SXRF) spectroscopy were used to evaluate metal distribution. Synchrotron techniques (μ-XANES, μ-EXAFS) along with infrared spectroscopy (DRIFT) were used to determine Mn speciation.
Results At lower Mn concentrations or when grown together with Ni, Mn is confined to the trichome basal compartment in the +2 oxidation state in a complex with phosphate. At tissue concentrations >1,150 μg g^{-1} Mn-rich lesions develop around some trichomes in which greater amounts of Mn^{3+} is found.
Conclusions Mn is preferentially stored in trichomes on the plant surface which at higher concentrations enters the cell wall or apoplastic space of neighboring cells resulting in the formation of brown reaction products and oxidized Mn species. We propose a mechanism by which lesion formation and oxidized Mn species around some trichomes is possibly due to induction of the peroxidase system by excess Mn, triggering the accumulation of toxic phenoxy radicals and Mn^{3+}.

Keywords Manganese (Mn) · *Alyssum murale* · Trichome · Hyperaccumulation · Nickel (Ni) · Synchrotron x-ray absorption fine structure spectroscopy (XAFS)

Responsible Editor: Fangjie Zhao.

Electronic supplementary material The online version of this article (doi:10.1007/s11104-013-2003-7) contains supplementary material, which is available to authorized users.

D. H. McNear Jr. (✉) · J. V. Kupper
Rhizosphere Science Laboratory, Department of Plant and Soil Sciences, N122S Agricultural Sciences North Building, University of Kentucky,
1100 Nicholasville Road, Lexington, KY 40546-0091, USA
e-mail: dave.mcnear@uky.edu

Introduction

Manganese (Mn) is an essential micronutrient for plants, protecting cells from oxidative stress as a component in oxygen radical scavenging enzymes (e.g. Mn superoxide dismutase (MnSOD)), a catalyst for enzymes such as decarboxylases and dehydrogenases, and is a key component of the water splitting system of photosystem II. The normal range of Mn concentrations in plant tissues varies widely from ~10 to 30 μg Mn g^{-1} leaf dry weight (d.w.) for most plants (e.g. soybean and corn) to over 1,000 μg Mn g^{-1} leaf dw for a few species (e.g. Pecan and Sugar Maple), while the critical toxicity limits for most crops occur above 500 μg Mn g^{-1} dw tissue (Macnicol and Beckett 1985; El-Jaoual and Cox 1998; Marschner 2012). Notably, the normal and critical toxicity concentrations differ within cultivars and due to a variety of climatic and edaphic factors. The large range of Mn content may be due in part to evolutionary adaptation of plants to large fluctuations in Mn

availability in soils brought about by frequent swings in redox conditions (Reeves and Baker 2000; Marschner 2012).

Abiotic stresses are the primary cause of crop losses, especially in the case of Al and Mn in highly weathered acidic soils, which can result in yield reductions of more than 50 % (Bray et al. 2000). Mn toxicity is a common cause of yield and growth reduction in agricultural crops such as soybeans, wheat, barley and oats and in natural ecosystems (El-Jaoual and Cox 1998). Ninety-nine percent of Mn enriched soils occur naturally, having been derived from Mn enriched parent materials, while the remainder results from atmospheric deposition of fossil fuel combustion and industrial activities as is the case for areas of the Northeastern U.S. and Europe (Herndon et al. 2011).

There are two prevailing mechanisms plants have been shown to use to tolerate high shoot Mn concentrations. The first mechanism is compartmentalization of Mn primarily into vacuoles or other compartments where it will not interfere with vital plant processes (Pittman 2005; Fernando et al. 2012). The second mechanism is the distribution of Mn within the apoplastic space or bound to the cell wall (Horst 1988). Plants respond to Mn toxicity in a variety of ways the most common being the development of brown or black spots on the leaf surface most often attributed to the oxidation of Mn^{2+} and phenolic compounds to more reactive and toxic Mn^{3+} and phenoxyl radical forms, respectively (Fecht-Christoffers and Horst 2005).

Interestingly, there are several plants in which Mn and other metals are preferentially stored in trichomes. Trichomes are glandular or non-glandular, single or multi-cellular, often calcium-rich hairs covering the shoot surface with a wide variety of morphologies and are generally used to protect the shoot from insect predation, intense sunlight, or high temperatures (Werker 2000). In plants from the Brassicaceae family (like *Alyssum murale*), non-glandular trichomes are always comprised of only a single cell while glandular trichomes are almost always multicellular. *Alyssum murale* only has non-glandular trichomes which are strongly correlated with plants from arid habitats (Beilstein et al. 2006; Beilstein et al. 2008).

Several studies have evaluated metal accumulation in trichomes. In tobacco exposed to excess Cd, Cd and Ca containing crystals were identified in the heads of tall and short trichomes (Choi et al. 2001; Choi et al. 2004; Harada and Choi 2008). In a later study the precipitates were identified as Cd substituted calcite ($CaCO_3$) and vaterite (μ-$CaCO_3$) (Isaure et al. 2010). Similarly, Zn was found to be incorporated into calcite, and Cd into calcite and vaterite crystals in the head cells of tobacco trichomes when taken up at toxic concentrations (Sarret et al. 2006; Sarret et al. 2007).

Much less is known about the speciation of Mn in trichomes. Sunflower, when exposed to high levels of soluble Mn, is known to take up large amounts (>7,000 mg kg^{-1}) where much of it was found to be preferentially stored in and around trichomes on the lower stem and petioles in a form where it is not able to cause toxicity to cytoplasmic biochemistry (Blamey et al. 1986). Horiguchi (1987) examined Mn accumulation in rice, barley, alfalfa, cucumber and pumpkin and found only cucumber to accumulate Mn around shoot trichomes in an oxidized form. Mn tolerance in each of these studies was attributed to the sequestration of oxidized Mn in the trichomes.

The Ni hyperaccumulating plant *Alyssum murale* was also found to preferentially accumulate Mn in the base and around trichomes on the leaf surface (Broadhurst et al. 2004b; McNear et al. 2005; Broadhurst et al. 2009). Mn accumulation in other Ni hyperaccumulating Brassicaceae species are reported in the range of 20–150 μg g^{-1} when grown in natural ultramafic soils (Tumi et al. 2012; Bani et al. 2010). Broadhurst et al. (2004b) found ~800 μg Mn g^{-1} shoot in *A. murale* 'Kotodesh' grown in a serpentine soil from Oregon (Typic Xerocherepts) containing ~3,800 mg Mn kg^{-1} (or ~70 mmol Mn kg^{-1}) (Kukier et al. 2004). It should be noted that the serpentine soils used in the Kukier et al. (2004) study were dried prior to being used which has been shown to increase Mn availability and likely resulted in the higher Mn concentrations in those plants. Broadhurst et al. (2004a) also found, in a study examining Ni uptake in *A. murale* grown in soils increasingly enriched with Ni, that the Kotodesh ecotype accumulated from 90 to 740 μg Mn g^{-1} shoot (dry weight) with no apparent correlation with exogenous Ni concentrations. In a later study examining the interaction between Mn and Ni in *A. murale* Broadhurst et al. (2009) showed that Mn content increased with increasing Mn additions to plants growing in Mn-spiked Promix™, reaching a maximum of 597 μg Mn g^{-1} in the 10 mmol Mn kg^{-1} Promix™ (~550 mg kg^{-1}) treatment. *Alyssum murale* has adapted to growing in serpentine soils which are naturally enriched with Mn possibly leading to higher Mn tolerance.

Manganese in *A. murale* was found to accumulate in the basal compartment of the trichome in the +2 oxidation state based on XANES data from one trichome base, however the chemical form was not determined (Broadhurst et al. 2009). In order to better understand the mechanisms of trichome-specific Mn accumulation and lesion formation, the objective of this study was to evaluate the effects of a range of Mn concentrations on plant growth, Mn accumulation, as well as the pattern of compartmentalization and speciation of Mn in and around trichomes of the Ni hyperaccumulator *Alyssum murale*.

Materials and methods

Plant growth

Vegetative cuttings (~ 10 plants/treatment) from mother plants of the 'Kotodesh' accession (from Albania) of the Ni hyperacumlator *Alyssum murale* (Waldst. & Kit.) were grown using EZ-Clone 30 (EZ Clone, Sacramento, CA) aeroponic chambers in a greenhosue. Plants received light for 16 h each day using a combination of high pressure sodium vapor lamps and natural sunlight. Day/night temperatures were approximately 25 °C and 21 °C, respectively. A minimal nutrient solution was used containing the following constituents: 0.6 mM K_2SO_4, 0.2 mM $MgSO_4$, 25 μM H_3BO_3, 0.50 μM $ZnSO_4$, 0.5 μM $CuSO_4$, 0.5 μM Na_2MoO_4, 0.02 μM $CoCl_2$, 0.5 mM $CaCl_2$, 2.0 mM NH_4NO_3, 50 μM EGTA, 0.3 mM KH_2PO_4 and 5 μM Fe-N,N-Di-(2-hydroxybenzoyl)-ethylenediamine-N,N'-diacetic acid (Fe(III)-HBED). Fe(III)-HBED was used to avoid non-specific interactions with the Fe chelator and target metals (i.e. Mn and Ni) as has been shown to occur with other Fe chelators (Chaney 1988). The pH of the nutrient solution was buffered to 6.1 with 1.0 mM 2-(N-morpholino)-ethane sulfonic acid (MES). Combinations of Ni (0.125 and 50 μM) and Mn (0.2, 5, 10, 20, 30, 50 μM) treatments as delineated in Table 1, were achieved by adding them to the nutrient solution from sulfate salt stock solutions ($MnSO_4$, $NiSO_4$). Nutrient solutions were modeled using GEOCHEMEZ which showed a −log Mn free activity ranging from 7.377 to 4.786 for the continuum of treatments from 0.2 μM to 50 μM Mn. Control plants were grown in solutions containing 0.125 μM Ni and 0.2 μM Mn. Nutrient solutions were changed weekly.

Total metal analysis

Plants were grown for 28 days after which they were removed from the aeroponic chambers, roots rinsed with 0.001 M $CaCl_2$ to remove any non-specifically sorbed Mn, divided into leaves, stem and roots, shock frozen in liquid nitrogen, freeze dried and weighed in preparation for total metal analysis. Leaf, stem and root materials from each plant were ground using an agate mortar and pestle and three equal aliquots were microwave digested following EPA method 3052 in a MARSXpress system (CEM, Matthews, North Carolina). After every 20th sample, one sample duplicate, blank and standard reference material (apple leaf NIST # 1515) were digested and analyzed to account for matrix effects, carry over and metal recovery, respectively. After sufficient dilution total metal contents in the digestates were determined using an Agilent 7500 series ICP-MS (Santa Clara, Ca). An internal yttrium standard was added to all samples to correct for instrument drift and other errors. The concentration of Mn in the shoot relative to the root (translocation factor; T*f*) was calculated as follows:

$$Tf = \frac{((\mu g\ \ g^{-1}\ \ \text{Mn leaf} \times \text{leaf}\ \ \text{wt.(g)}) + (\mu g\ \ g^{-1}\text{Mn stem} \times \text{stem}\ \ \text{wt.(g)})(\text{leaf}\ \ \text{wt.(g)} + \text{stem}\ \ \text{wt.(g)})^{-1}}{\mu g\ \ g^{-1}\text{Mn}\ \ \text{root}}$$

Electron probe micro-analysis (EPMA)

Plant samples were prepared by immersing whole sections of shoot in liquid nitrogen after which they were dried under vacuum at −80 °C for 24 h. Leaves were then placed on a carbon stub and sputter coated with a 2–3 nm of gold. Samples were examined on a Model S-3200 Hitachi scanning electron microscope equipped with a Princeton Gamma-Tech Energy Dispersive Spectroscopy (EDS) microanalysis system. Samples

were first scanned manually from 50–300× magnification using backscattered electron (BSE) imaging to find regions of high Mn concentration after which EDS was used to generate elemental maps for C, Ca, Mn, P, S, Cl, K and O.

μ-SXRF, μ-XANES and μ-EXAFS data collection and analysis

Micro-EXAFS and μ-synchrotron x-ray fluorescence (μ-SXRF) data were collected on beamline 10.3.2 (1.9 GeV and 500 mA) at the Advanced Light Source, Lawrence Berkeley National Lab (Berkeley, CA) (Marcus et al. 2004). Leaves were removed from living plants mounted on a square of Mo foil using silicon vacuum grease, plunged in liquid nitrogen and mounted directly to a Peltier cold stage maintained at∼−30°C. The sample stage was then oriented 45° to the incident X-ray beam. Fluorescence signals were collected using a Ge solid-state multi-element detector. To assess the spatial distribution of Mn and other elements in the samples, fluorescence maps were collected over 1,000 μm^2 (coarse map) and 200 μm^2 (fine map) with a beam size of 16×7 μm and 5×5 μm, respectively, using a step size of 20 and 5 μm and an integration time of 100 ms. For mapping, the beam energy was set to 11 keV to allow the detection of Ni, Fe, Ca, Co, Cu, Zn, and Mn. To determine Mn speciation at regions of interest in the maps, μ-XANES and μ-EXAFS spectra were collected up to 300 eV or 500 eV, respectively, above the Mn K-edge. A total of 8 leaves were analyzed from multiple plants via XAS from which about 5–20 μ-XANES and μ-EXAFS spectra were collected, processed and averaged per point. Prior to μ-XAS data collection, the beamline energy was calibrated to the first inflection point of the Mn metal foil standard (E_o=6.539 keV). Data were then processed and fit using standard methods as described in supplementary online information.

There is insufficient published research directly addressing the influence of plant sample preparation methods for synchtrotron based analysis on metal distribution and speciation in plant tissues. The majority of studies using synchrotron techniques use methods of tissue preparation similar to those described in this study (Freeman et al. 2007; Fernando et al. 2010; Quinn et al. 2011; Sarret et al. 2009; Isaure et al. 2006). Notably, Fernando et al. (2010) and Isaure et al. (2006) in synchrotron-based studies on Mn in *Chengiopanax sciadophylloides* and Cd in *Arabadopsis. Thaliana*, respectively, provided a thorough comparison of sample preparation techniques (freeze-drying vs. fresh-frozen tissue), both concluding that no changes in speciation or distribution had occurred. Collection of spectra and maps at ALS beamline 10.3.2 is always done with great care. Each spectrum is compared as they are collected to check that no beam induced changes have occured. If damage is detected, the spectrum is discarded and another spot is selected for analysis. In this study several orthogonal methods (μ-SXRF, SEM, light microscopy) were used and cross-referenced to confirm that redistribution didn't occur due to sample preparation.

Diffuse reflectance infrared Fourier transform (DRIFT) spectroscopy

A 5 % mixture of shock frozen and freeze dried leaf tissue from each of the treatments was prepared by grinding and thoroughly mixing it with an aliquot of spectroscopy grade potassium bromide (KBr). Samples were then analyzed on a Thermo-Fisher Noclet 6700 Fourier transform infrared spectrometer equipped with a Smart Collector diffuse reflectance accessory and MCT/A detector. For each sample, 254 spectra were collected with 4 cm^{-1} resolution.

Results

Plant growth and Mn uptake and translocation

Nutrient solutions containing 5 and 10 μM Mn had a stimulatory effect on whole plant growth relative to the control ([Mn]=0.20 μM) resulting in a 2–3 fold increase in whole plant weight (Fig. 1). Beyond 10 μM Mn plant weight dramatically decreased reaching a minimum in the Ni_{50}/Mn_{50} treatment (Supplemental Online information Fig. S1). Maximum whole plant Mn concentrations were found in the Ni_0/Mn_{30} and Ni_0/Mn_{50} treatments (~2,800 μg g^{-1} for each), but were accompanied by a significant reduction in shoot, root and whole plant mass (Fig. 1, Supplementary Online Information Table S1 and Fig. S1) and visible toxicity symptoms (Mn only treatments) on the leaves (Mn spots, see Figs. 5b and 6) and stems. Throughout all treatments leaves appear to be the primary repository for Mn, although, at Mn concentrations beyond 20 μM the contribution of Mn in the stem to the total shoot Mn concentration becomes much higher (Fig. 1 and Supplementary Online Information

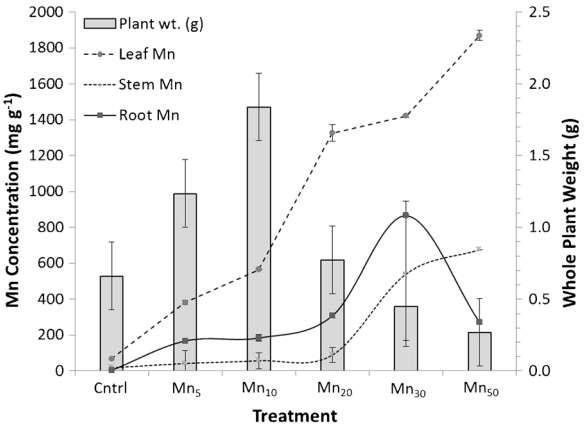

Fig. 1 Relationship between total Mn concentration (lines, primary axis) in stem, root and leaf tissues and whole plant weight (gray bars secondary axis) of plants grown in nutrient solutions supplemented with varying μM amounts of Mn (Cntrl=0.2 μM Mn)

Table S1). There is little correlation between increasing Mn concentrations and the concentrations of the other elements analyzed (Table S1). Notably, Ca concentrations peaked in the Mn_{10} treatment and there was significantly less Ca in the plants receiving the Ni only treatment (Ni_{50}/Mn_0) compared to any other treatment.

The T*f* provides an indication of the relative efficiency of metal uptake. The T*f* for the control treatment were 14.4 providing a baseline for Mn translocation and storage in *A. murale* (Supplementary Online Information Fig. S2). At 5 μM Mn solution concentrations there is a significant decrease in the T*f* relative to the control (1.6 vs. 23) after which there is an upward trend in Tf (Supplementary Online Information Fig. S2). An exception is the 30 μM treatment where there was a significant dip in the T*f* coinciding with the maximum root associated Mn, Fe, Ni and Ca concentrations (Supplementary Online Information Table S1) after which the T*f* rapidly increased. Interestingly, in the treatment receiving 50 μM Ni the Mn T*f* was proportional to that observed for the 20 μM Mn treatment. More Mn remained in the roots in the Ni only treatment along with Zn (~504 μg g^{-1} vs. ~149 μg g^{-1}) and Fe (~178 mg g^{-1} vs. ~34 mg g^{-1}) (Supplementary Online Information Table S1) compared to the control or the 50/50 μM Ni/Mn treatment. When 50 μM Ni is present together with the same amount of Mn there is a significant increase in the Mn T*f*, however unlike in the Ni only treatment, the Fe concentrations in the root are similar to that of the control.

Metal distribution and compartmentalization

The trichomes on *A. murale* are Ca-rich, unicellular, multi-branched (stellate), non-glandular structures with small nodules covering the rays (Fig. 2). When Mn is present alone and at high available concentrations in the growth solution, a variety of patterns emerge associated with the trichomes ranging from Mn in the center (Fig. 2c), within the rays (Fig. 2f), in the outer portions of the rays (Fig. 2a, d, e), no Mn at all (Fig. 2b) or Mn emanating out from the trichome into the surrounding tissues forming Mn rich lesions (Figs. 5b and 6a-d). Multi-channel analysis of points in the center and rays of a trichome (Fig. 3 points 1 and 2) from a plant grown in 50 μM Mn reveal the dark black or brown bands in the light microscope images (Fig. 2a, d, e) are enriched in Mn. Several other metals were colocalized with Mn in the trichome rays (Fig. 3). Ca was by far the most abundant element in the trichome followed by Mn>>Fe>Ti>Ni. The potassium (K) SXRF map in Fig. 3 is indicative of the vasculature of the plant in which it appears that several veins are converging where the trichome is located on the leaf.

Interestingly, when Mn is present at lower available nutrient solution concentrations (<20 μM Mn) or in conjunction with Ni the black lesions around the trichomes did not seem to form and Mn is contained within the trichome most notably at the base (arrows Fig. 5a). The SEM EDX maps of a leaf cross-section with trichome from the 10 μM Mn treatment shows the discrete concentration of Mn within the basal compartment of the trichome in close association with P (Fig. 4b). Analysis of several spots around and on the trichomes using EDX point analysis (Fig. 4a points 1–4) showed that tissues surrounding the trichome (point 1) and within the central part of the trichome rays (point 4) had no detectable Mn, while the basal compartment (Point 2) had greater amounts of both Mn and P with much less Mn detectable further up the trichome (Point 3).

μ-XANES, μ-EXAFS and DRIFT spectroscopy determination of Mn speciation

There is a slight dampening and widening of the absorption edge peak in the spectra from spots 3 and 4 compared to those from spots 1 and 2 (Fig. 7). Linear combination fits (LCF) for spots 1 and 2 are dominated by hureaulite (~63–70 %) followed by Mn citrate (~20–

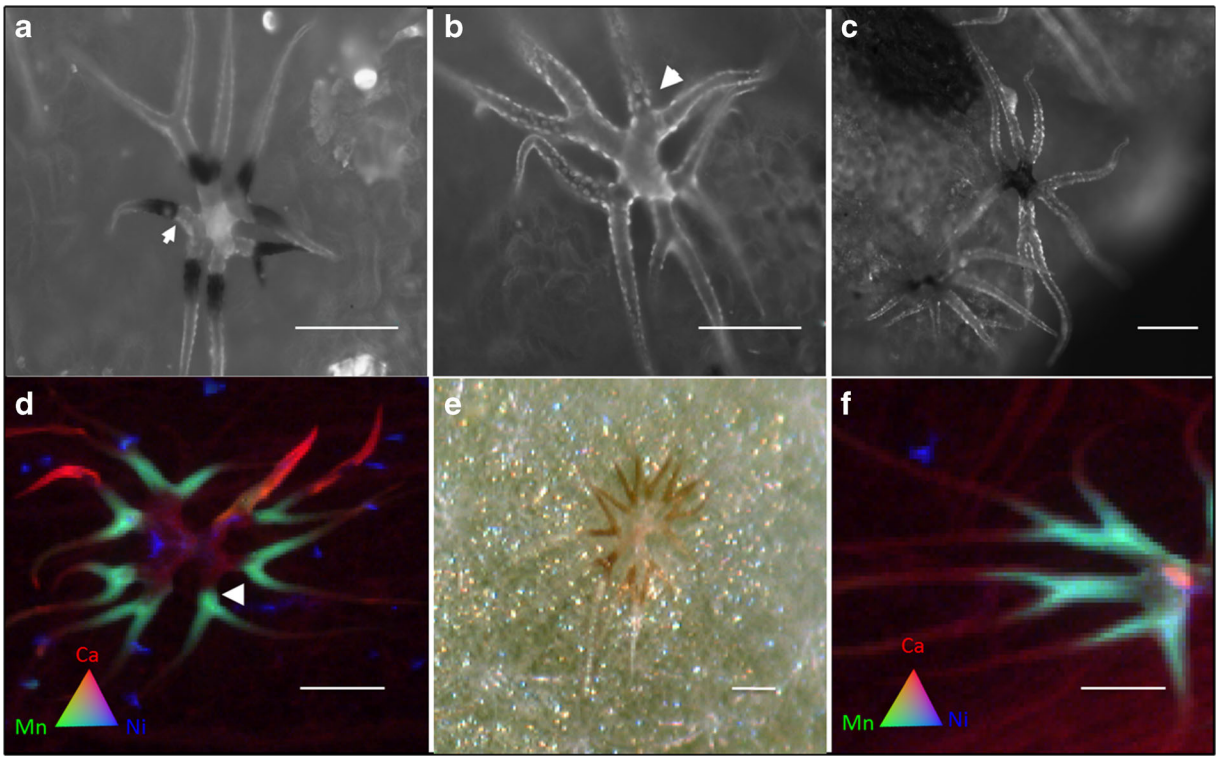

Fig. 2 Light microscope (a–c and e) and μ-SXRF (d and f) images of leaf trichomes from *A. murale* grown in a nutrient solution containing 50 μM Mn. *Bar* in all figures represents 100 microns

30 %) with lesser amounts (~7–10 %) of the Mn^{3+} and mixed Mn^{2+}/Mn^{3+} standards manganite and hausmannite, respectively. Spot 3 is primarily composed of $MnSO_4$ with the balance comprised of the Mn^{3+} and Mn^{2+}/Mn^{3+}, manganite and hausmannite standards (~26 and 15 %, respectively). Spot 4 which is closer to the trichome, has near equal proportions of Mn Citrate (~37 %), hureaulite (~33 %) and the Mn^{2+}/Mn^{3+} standard hausmannite (~30 %). Least squares fits of the μ-EXAFS spectrum collected from spot 1 were best fit with Mn coordinated to 6 O atoms in the first shell at 2.15 Å and 2.9 P atoms in the second shell at 3.34 Å (Fig. 8). The first coordination shell of Mn in hurealite, the dominant species identified at spot 1 and 2, is made up of 6 O atoms (i.e. octahedral coordination) in the first shell at 2.16 Å. In the second shell Mn is coordinated with 6 phosphorus atoms from the phosphate groups at an average distance of 3.45 Å. Linear combination fitting estimated ~70 % hureaulite at spot 1 in which case, if taken literally, we would expect the $CN_{Mn\text{-}P}$ to be about 4.2 (i.e. 0.7×6=4.2). The lower than expected $CN_{Mn\text{-}P}$ in the fit (2.9) may be due to destructive interference from Mn in the Mn-Mn edge-sharing octahedra (as is present in hurealite) found at a similar distance as the Mn-P shell. Adding to this, the material is more than likely highly disordered making it impossible to get good estimates of the Mn-P coordination number. Regardless, the coordination and bond lengths for O and P are consistent with those found in hureaulite and at the very least support the presence of a Mn-P second shell. Best least squares fits of the μ-EXAFS spectra from spot 3 were achieved with only one oxygen shell comprised of 5.1 atoms at 2.16 Å which is supported by the LCF of the μ-XANES data where the dominant Mn species was found to be Mn sulfate in which Mn is in octahedral coordination (Fig. 8).

The near-IR features at ~1,655 cm^{-1} and 1,542 cm^{-1} are characteristic of the C=O stretching mode of amide I and the N-H deformation of amide II, respectively, and remain virtually unchanged with treatment (Fig. 9). The peak at ~1,736 cm^{-1}, likely due to C=O stretching from acetyl group containing polysaccharides in the plant tissues, also remains unchanged with treatment. The peaks at 1,430 cm^{-1} and 1,389 cm^{-1} along with the peaks at 1,149 cm^{-1}, 1,078 cm^{-1}, and 1,054 cm^{-1} proved to be the most sensitive to the Mn treatments

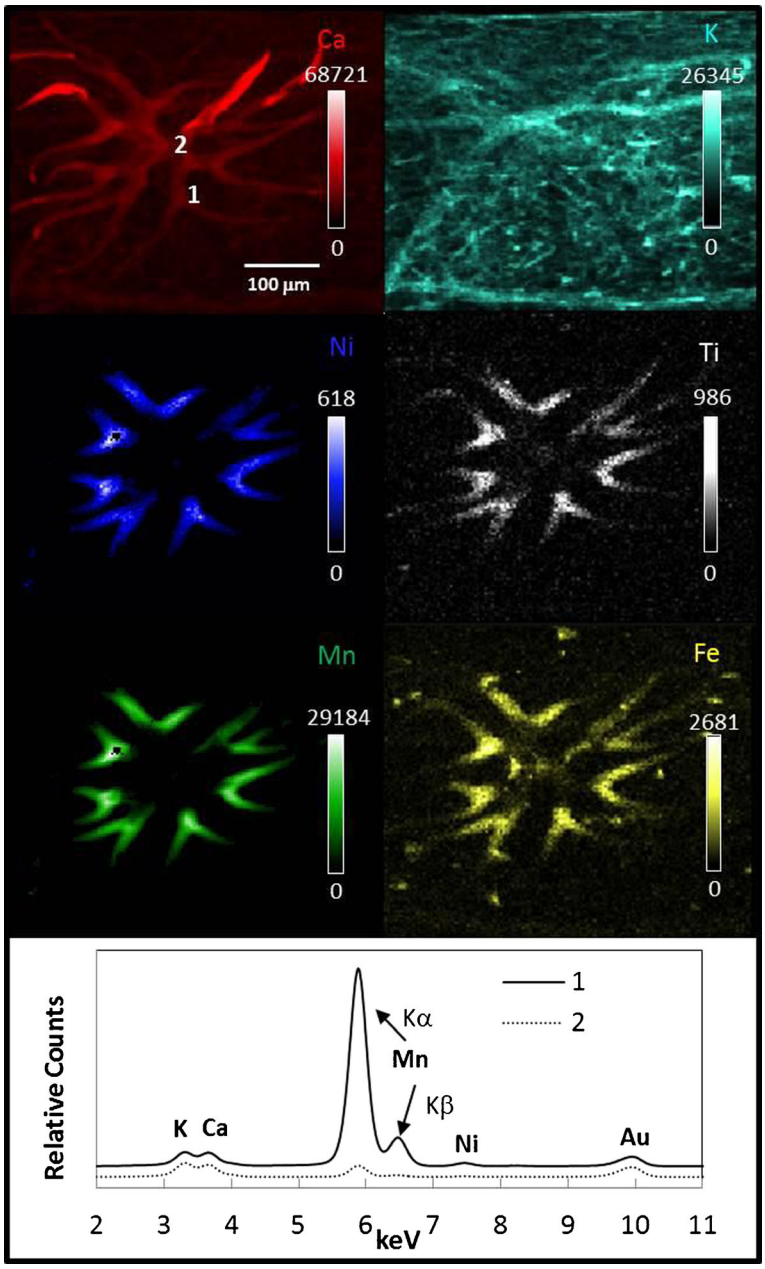

Fig. 3 µ-SXRF maps showing the distribution of Ca (*red*), K (*aqua*), Ni (*blue*), Ti (*white*), Mn (*green*) and Fe (*yellow*) in and around a trichome on an leaf from *A. murale* grown in 50 µM Mn. Bottom panel shows a multi-channel spectra from points 1 and 2 shown in the Ca µ-SXRF micrograph

and are indicative of the O-H bending and C-O stretching modes of alcohols and/or phenols. The spectra for the control, 5 µM and 10 µM Mn treatments remain virtually unchanged. In the 20 µM and 30 µM Mn treatment the peaks at 1,430 cm^{-1} and 1,389 cm^{-1} are considerably dampened. In the 50 µM Mn treatment the 1,389 cm^{-1} peak broadens and shifts to 1,365 cm^{-1}. With the addition of 50 µM Ni together with 50 µM Mn the 1,389 cm^{-1} peak remains shifted to 1,365 cm^{-1} and is broader. The spectrum for the 50 µM Ni-only treatment is no different than the control, 5 µM or 10 µM treatments.

Discussion

Mn content in A. murale

Under the conditions of this study, the 'Kotodesh' ecotype of *Alyssum murale* accumulated more Mn than has

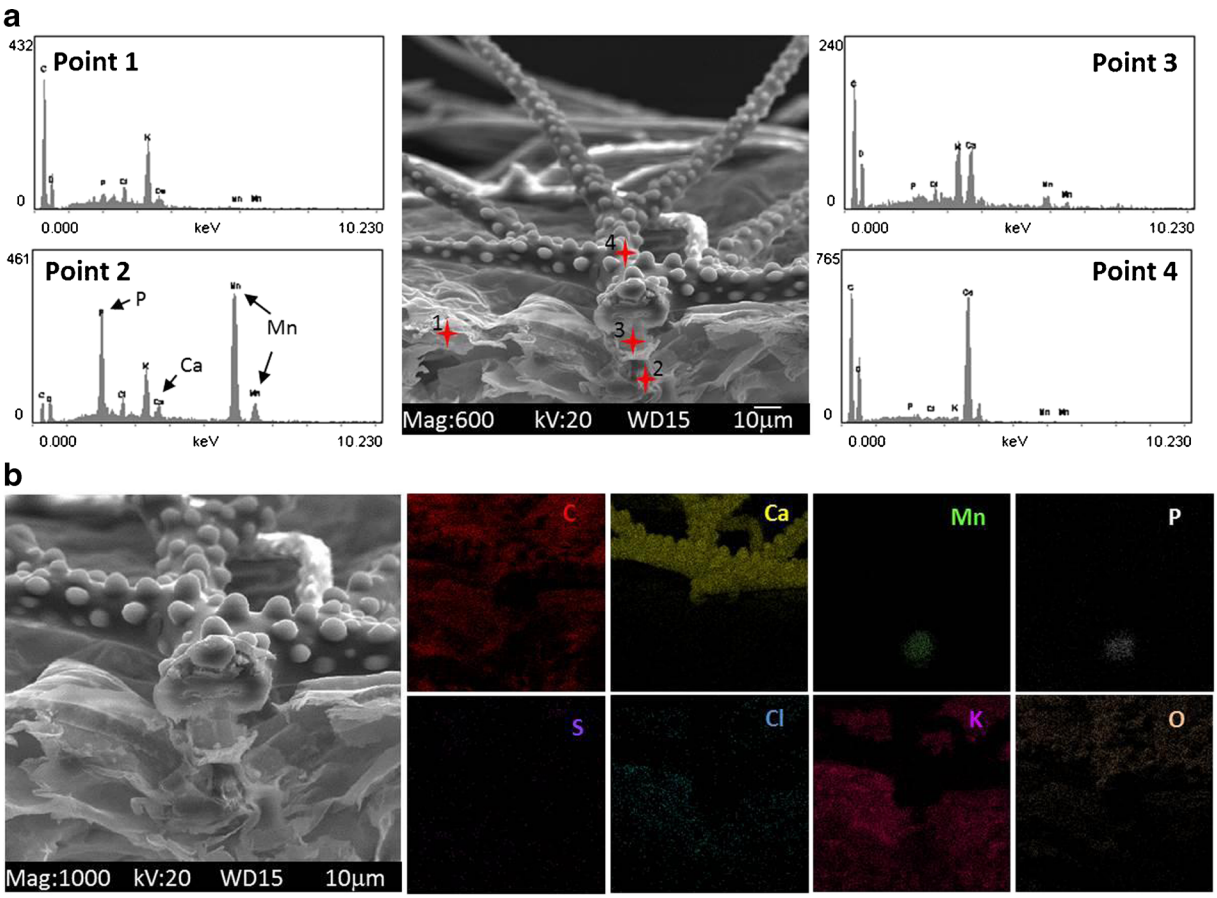

Fig. 4 Backscattered electron (BSE) image of a trichome from *A.murale* grown in 10 µM Mn and the accompanying energy dispersive x-ray (EDX) spectra from points 1–4 shown in the BSE image (**a**). Enlarged BSE image of the trichome and EDX elemental maps showing the distribution of C, Ca, Mn, P, S, Cl, K, and O in *A. murale* grown in 10 µM Mn (**b**). Note the colocalization of Mn and P

been reported in most investigations of Alyssum species to date. In *A. murale,* Mn associates exclusively with the trichomes covering the leaves and stems (Figs. 2, 3, 4, 5, 6 and 7), only entering the apoplastic space or cell wall at higher Mn concentrations (Fig. 6). Preferential accumulation of Mn in trichomes is similar to what has been observed in sunflower, cucumber, tobacco and stinging nettle where the deposition of manganese oxides was considered a tolerance mechanism (Blamey et al. 1986; Horiguchi 1987). Sarret et al. (2002 and 2009) examining the Zn distribution in the Zn hyperaccumulator *A. halleri* observed multiple metals accumulating in trichomes. Based on the µ-SXRF and SEM micrographs from their studies, Zn along with Mn was found in a ring around the base of the trichome (similar to the ring distribution in this and other studies) with Mn extending further up into the trichome stalk. Notably, the distribution of Mn in the trichome stalk in their studies appears well correlated with P (e.g. see Figs. 9 and 11 of Sarret et al. 2009).

In our plants grown in the Mn_{10} treatment we found Mn accumulated primarily in the basal compartment of the trichome in association with phosphorus (Fig. 4b). Colocalization of Mn and P in the root and shoot tissues as P and Ca rich granules has been observed in Douglas fir exposed to excess Mn and was attributed to the enhanced tolerance of some Douglas fir species (Ducic and Polle 2007; Ducic et al. 2012). Exposure of sorghum to excess Mn was also shown to increase shoot concentrations of phosphorus (Galvez et al. 1989) and in Pokeweed (*Phytolacca americana*) Mn and P rich crystals were observed and presumed to account for the accumulation and detoxification of Mn in that plant (Dou et al. 2009). Broadhurst et al. (2009) observed S

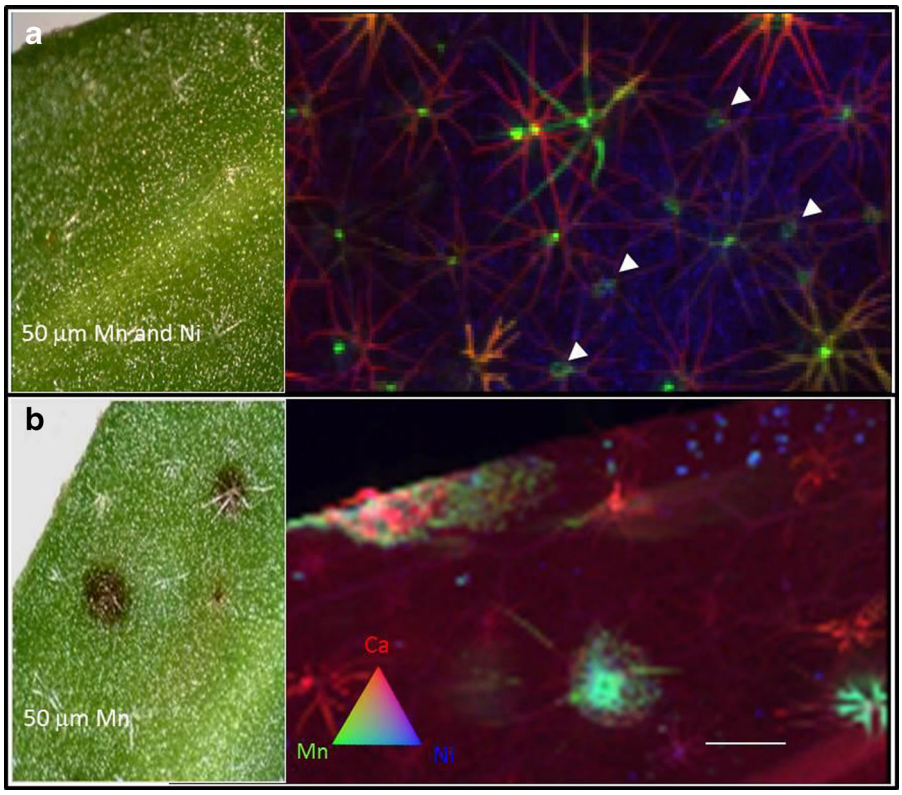

Fig. 5 light microscope images and µ-SXRF maps from *A. murale* plants grown in **a** 50 µM Mn and Ni and **b** 50 µM Mn alone. Note the difference in Mn distribution and the relative absence of the black Mn rich lesions in the Mn and Ni exposed plants

along with Ni and Mn in the basal compartment of trichomes on *A. murale* grown with excess Ni. They attributed the presence of S to sulfate (SO_4^{2-}) being used as a counterion in the vacuole. We did identify $MnSO_4$ using XANES in a necrotic lesion around one of the trichomes we probed but not in the trichome base, therefore, from our results it appears that the accumulation of S in the trichome may be linked primarily to Ni accumulation not Mn.

The concentration of Mn and Ca in *A. murale* trichomes are several orders of magnitude greater than in the surrounding cells implying a more deliberate loading of these metals (Fig. 3). In a previous study we found a mean Ca concentrations of >9 % dry leaf weight (McNear et al. 2005) with reports in trichome rays and nodules on the rays exceeding 30–50 % (Broadhurst et al. 2004b). Broadhurst et al. (2004a) using SEM found Ca, C and O concentrations in trichomes of *A. murale* consistent with calcium carbonate with Tappero (2008) later confirming, using synchrotron XRD, that trichomes are composed of calcium carbonate. There is one report in which Ca in trichomes of Brassica species was found to be concentrated in the highly bifringent cell walls as calcium carbonate (Erisymum spp.) or calcium phosphate (*A. thaliana*) (Webb 2007). Calcium concentrations were so high in trichomes that some have postulated a functional role for these cells in regulating Ca concentrations within plants (Braodhurst et al. 2013; De Silva et al. 1996). However, Ca storage in plants for later use usually occurs as amorphous calcium carbonate, an often transient, precursor form of Ca, which can transform to more stable crystalline calcium carbonate minerals or is stabilized into structures for mechanical purposes.

While the production of trichomes for maintaining Ca homeostasis is one possibility for *A. murale*, there are many functions attributed to trichomes (Wagner et al 2004) with much stronger evidence that trichomes have evolved to protect plants from insect herbivory (Levin 1973; Southwood 1986; Ågren and Schemske 1994; Karban and Baldwin 1997; Traw and Dawson 2002), and importantly improved drought tolerance by limiting the absorbance of solar radiation (Ehrlinger 1984; Choinski and Wise 1999; Benz and Martin 2006) and

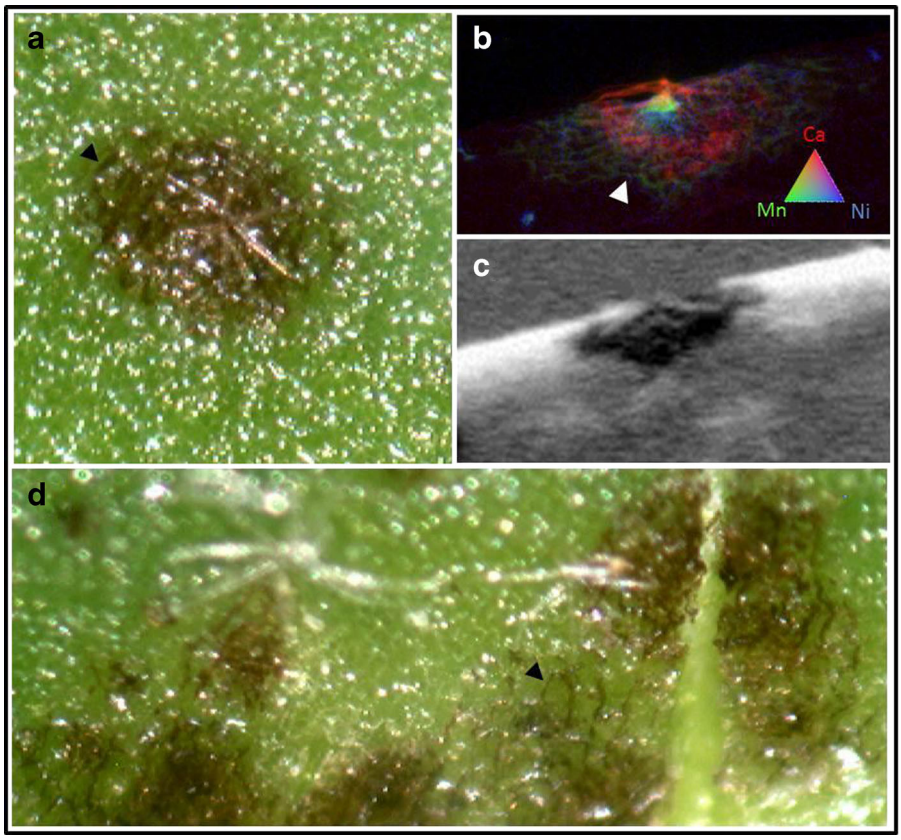

Fig. 6 Light microscope images (**a**, **c** and **d**) and μ-SXRF micrograph (**b**) of Mn lesions on freshly removed leaves from *A. murale* plants grown in 50 μM Mn. *Black and white arrows* in a, b and d highlight Mn deposits in the cell walls or apoplastic space

increasing the condensation of moist air at the leaf surface (Jeffree 1986). *Alyssum murale* only has non-glandular, stellate trichomes which have been strongly correlated with plants from arid habitats (Beilstein et al. 2006). Therefore, the primary driver for the evolution of *A. murale* trichomes may be protection from the intense heat and dry conditions found in the Mediterranean region they originated from. Further, the use of Ca for trichome construction is not unique to hyperaccumulating plants, but instead is found in many plants (Werker 2000) and its use as a fundamental building-block for all kinds of protective structures is seen throughout nature (Levin 1973).

Irrespective of the evolutionary reasons for trichome morphology and development, it is conceivable that these cells would have a larger demand for Ca, and thus, the cellular apparatus in place to meet that demand. One of the primary controllers of Ca in plant cells are the cation exchanger family proteins (CAX), specifically the cation/H+CAX1 and CAX2 genes, which encode proteins responsible for transporting Ca and Mn, respectively (Schaaf et al. 2002; Pittman 2005). Importantly, CAX2 has been strongly localized to the vasculature of plants and is postulated to play an important role in mediating the loading and unloading of Mn into plant vacuoles (Pittman et al. 2004; Pittman et al. 2005). Other versions of CAX genes have been identified in rice (e.g. OsCAX1a) and show high levels of expression in stomata and importantly trichomes (Kamiya et al. 2005; Kamiya et al. 2006). It seems likely that the preferential loading of Mn into the trichome is due in part to the ability of CAX family genes to encode proteins involved in the transport of both Ca and Mn, although further study is necessary to confirm this speculation.

Unlike previous studies of *A. murale*, in some trichomes we observed Mn not only in the trichome basal compartment but also further up in the trichome rays (Figs. 2 and 3). Interestingly, each ray of the trichomes in *A. murale* has what appears to be a distinct physical delineation (arrows in Fig. 2a,b and d) separating each ray from the trichome stalk. Many times Mn (along with

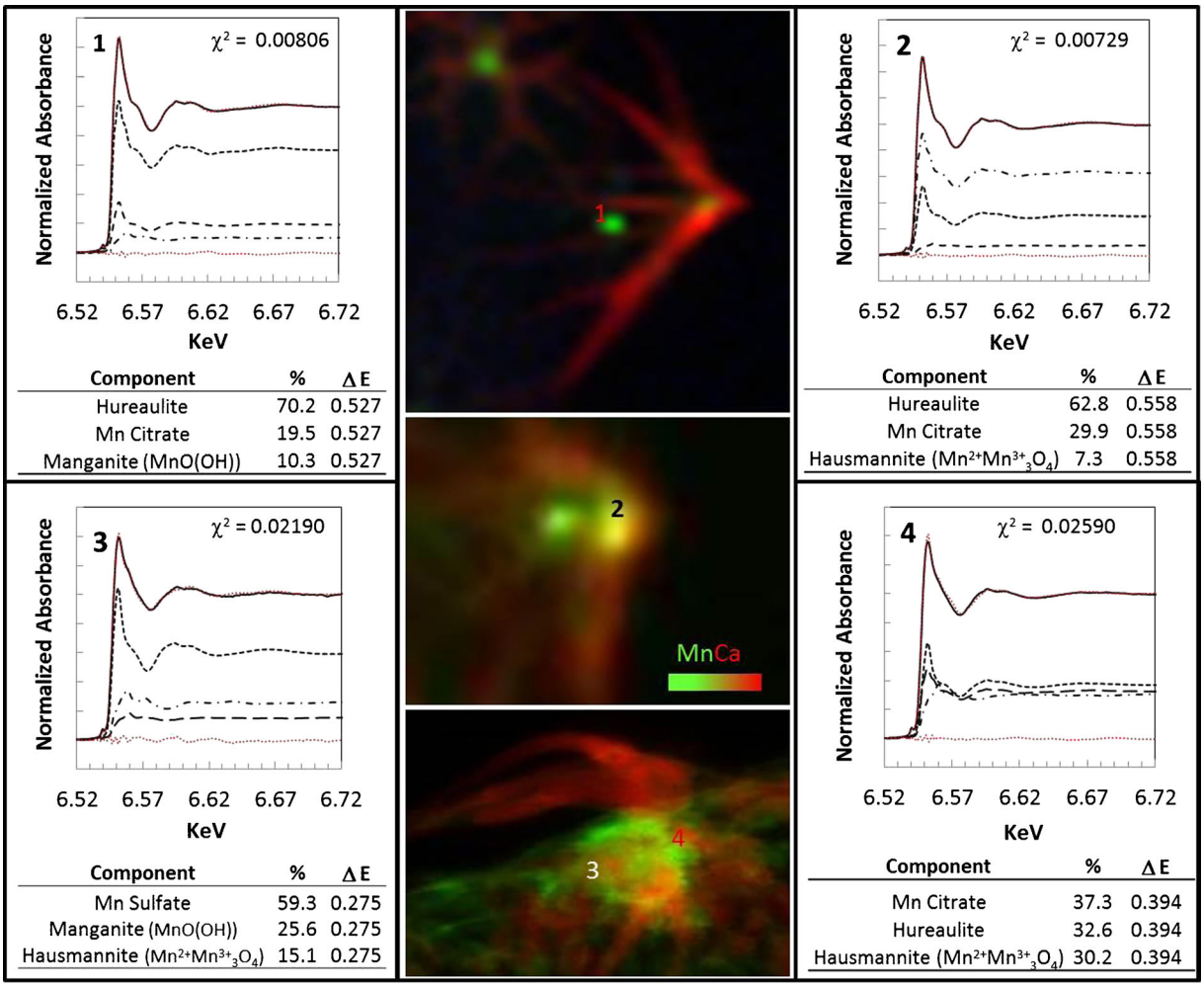

Fig. 7 Best linear least squares fits (LLSF) of μ-XANES spectra collected from spots 1–4 as shown in the μ-SXRF micrographs from three trichomes on plants grown in 50 μM Mn. The solid black line is the normalized spectrum and the overlaid red dotted line the best fit achieved using a combination of three standard spectra shown in the table below each fit. The intensity of the three standard spectra beneath the normalized spectrum show the relative contribution of each to the overall fit in the order (*top to bottom*) shown in the table. The bottom red dotted line is the fit residual. $\chi^2=\Sigma[(\text{fit}-\text{data})/\varepsilon]^2/(N_{\text{data}}-N_{\text{components}})$

the other metals) is partitioned to the outer rays just at or above this delineation (Fig. 3) where it appears brown in the light microscope images (Fig. 2e). A TEM micrograph collected by Broadhurst et al. (2004a; Fig. 3) of a trichome cross-section from *A. murale* shows a physical restriction in the trichome and a thickening of the cell wall where the rays emerge from the stalk corresponding to where we see Mn and the other metals accumulating in our study.

There are no detailed studies on trichome formation in *A. murale*, however, insights can be gained by looking at other plants in the Brassicaceae family such as the model plant *Arabidopsis thaliana*. In Arabidopsis, trichomes form from differentiated epidermal cells and develop via endoreduplicaton of protodermal precursor cells which occurs several times, starting with the initiation of trichome elongation and occurring once for each branch (3 in the case of Arabadopsis). Cell elongation and endoreduplication events are controlled by reactive oxygen species (ROS) (Foreman et al. 2003). It may be that the presence of excess Mn in the cell at the time of trichome development may result in the formation and deposition of Mn oxides at these locations resulting from the cell-division-initiating burst of ROS. There is no literature that we could find discussing how metals present during plant cell ontogeny, specifically

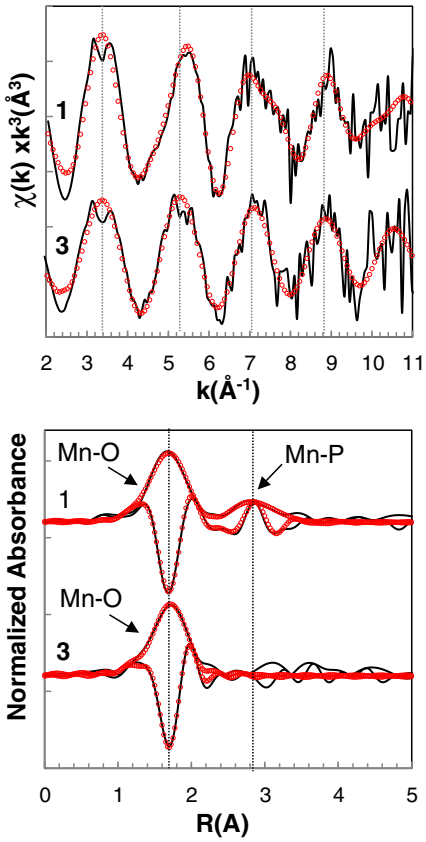

	Shell	N	R	σ^2	$\Delta E(eV)$	R
1	Mn-O	6.0	2.15	0.009	-0.25	4.6
	Mn-P	2.2	3.34	0.007	-	-
3	Mn-O	5.1	2.16	0.005	4.36	3.5

Fig. 8 Chi spectra (*top panel*) and radial stricture functions (*bottom panel*) from points 1 and 3 in Fig. 8 with best non-linear least squares fits (*red dotted lines*) achieved using parameters from the structural refinement of Hurealuite. Fit results are shown in the table at the bottom of the figure

the influence of ROS-initiated cell differentiation, may influence metal speciation, compartmentation and cycling. There are however, interesting parallels in other kingdoms such as fungi where, for example, Hansel et al. (2012) found that the fungus *Stillbella aciculosa,* when grown in the presence of soluble Mn(II), formed brown Mn(III/IV) oxides at the base of the fungal reproductive stalk (i.e. synnemata) in a pattern strikingly similar to what we observed at the base of trichomes on *A. murale.* They found that the Mn-oxides were formed as a result of fungal-derived ROS (i.e. superoxide) production during cell differentiation and development of the reproductive stalk.

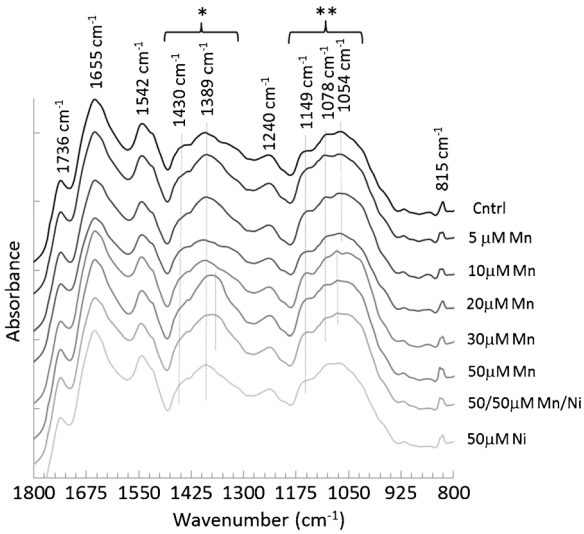

Fig. 9 Diffuse reflectance Fourier transform (DRIFT) infrared spectra from leaves of *Alyssum murale* grown in varying concentrations of Mn and Ni. * (1,430–1,330 cm^{-1}) indicates the O-H bending and ** (1,250–970 cm^{-1}) the C-O stretching of alcohols and/or phenols

Notably, not all of the trichomes on the leaf surface were equally enriched with Mn. Sarret et al. (2009) also found that not all of the trichomes on leaves of the Zn hyperaccumulaor *A. halleri* had Zn in them leading them to question whether this had to do with leaf age or the position of the trichome on the leaf. We observed, along with others (Broadhurst et al. 2009), that trichomes located closer to veins seem to contain more Mn compared to those not located on or near a vein. For example, the potassium μ-SXRF micrograph in Fig. 3 effectively shows the location of the leaf veins where ~5 veins can be seen converging where a trichome containing Mn and other metals is located.

Alternatively, unlike glandular trichomes, non-glandular trichomes are only functionally active in the early stages of development and once mature many are thought to become inactive and detached from neighboring cells (Ghasemi et al. 2009). So, maybe only those that are functionally-active later in leaf development continue to take up Mn. The distribution of functional and non-functional trichomes and their proximity to leaf veins may explain the variability in Mn distribution we observed, with some having Mn in the central stalk (Fig. 2c), in the rays (Fig. 2d, f) or no Mn at all (Fig. 2b). This variability may also explain why there is no clear consensus as to the role trichomes play in metal sequestration (Blamey et al. 1986; Kramer et al.

1997; Küpper et al. 2000; Psaras et al. 2000; Küpper et al. 2001). More analysis is clearly necessary to evaluate the influence of trichome morphology, ontogeny, proximity to leaf veins, and the role of CAX family (and other) transporters on the level and pattern of metal accumulation in the trichomes.

Mn speciation and the mechanism of toxicity

It appears that different mechanisms are responsible for the accumulation of Mn in the trichome base and rays than in the tissues forming the black lesions around the trichome. Manganese in the basal compartment of trichomes was identified by μ-XANES and μ-EXAFS as manganese phosphate mineral most closely resembling hureaulite ($Mn^{2+}{}_5(PO_3OH)_2(PO_4)_2 \cdot 4H_2O$) (Figs. 8 and 9). In pokeweed (*Phytolacca americana Linn*) Mn was found to form precipitates with P that the authors hypothesized play a role in Mn detoxification (Dou et al. 2009). Why Mn-P complexes are forming in the trichomes is still unclear, however there is some evidence that manganese phosphates can behave like superoxide dismutase by scavenging superoxide and protecting cells from oxidative damage. For example, Barnese et al. (2012) found that Mn phosphate and Mn carbonate complexes were effective at catalyzing the disproportionation of superoxide radicals at concentrations typically found in cellular systems (in their case, microbes). The correlation of Mn and P in this study and in others (Sarret et al. 2009) may therefore allude to the involvement of Mn in the non-enzymatic protection of these functionally unique cells from oxidative damage. Unfortunately, we were unable to collect quality XAS data on the trichome rays themselves to verify the form of Mn, although from the SEM EDX micrographs there is no correlation of Mn with P in the rays.

In and beyond the Mn_{20} treatment, Mn was found in the apoplastic space or cell wall (Fig. 6) resulting in visible necrotic lesions around trichomes on the stems and leaves (Figs. 5b and 6). At these locations oxidized Mn species (i.e. Manganite (MnOOH) and Hausmanite ($Mn^{2+}Mn^{3+}{}_3O_4$)) made up a greater proportion of the total Mn. We hypothesize that the specificity of Mn toxicity symptoms and lesion formation in the cells around trichomes in *A. murale* is due to the specific CAX-mediated loading of Mn to trichome cells. Continued Mn loading result in excess Mn in the trichome where it then begins to accumulate in the apoplastic space or walls of the surrounding cells. Mn stress has been shown to trigger the peroxidase system of the cell wall leading to an influx of phenolics into the apoplastic space which may either directly scavenge H_2O_2 or donate electrons to apoplastic peroxidases for H_2O_2 detoxification (Sakihama et al. 2002).

Wissemeier and Horst (1992) suggested that Mn may influence the production and compartmentalization of phenolics and (Fecht-Christoffers et al. 2006) concluded that the release of phenolic compounds into the apoplastic space in cowpea are responsible for modulating the H_2O_2 producing NADH peroxidase cycles primarily at advanced stages of Mn toxicity. The Mn induced oxidation of phenols catalyzed by the apoplastic POD system were shown to result in the production of phenoxy radicals and ultimately polypheonols which were attributed to the appearance of brown spots on the leaves characteristic of Mn toxicity in cowpea and other plant species (Wissemeier and Horst 1992; Fecht-Christoffers et al. 2003).

Mn in *A. murale* is well correlated with the visible brown reaction products in the leaf cell walls or apoplastic space likely because of the close links between phenol and Mn oxidation of the H_2O_2-POD system. Some authors have attributed Mn^{2+} oxidation to the buildup of H_2O_2 as the peroxidase system is overwhelmed by toxic Mn levels, however, H_2O_2 has not been shown to effectively oxidize Mn^{2+} (Hansard et al. 2011). Instead, it is hypothesized that the phenolic-ascorbate/H_2O_2 balance of the apoplast is exceeded resulting in the production of phenoxyl radicals and the likely persistence of other ROS (e.g. O_2^-, •OH, etc.) both of which are capable of oxidizing Mn^{2+} to Mn^{3+}. Linear combination fits of our XANES data show a higher amount of Mn^{3+} species in the Mn rich lesions along with mixed Mn^{2+}/Mn^{3+} oxides and Mn^{2+} complexed with organic ligands. If not stabilized by complexation or reduced by plant enzymes, more Mn^{2+} is oxidized to Mn^{3+} which in excess can act as a catalyst for the further oxidation of phenols, continuing the cycle of producing more polyphenols and phenoxy radicals. The reaction products act as strong oxidants of proteins and lipids resulting in cell damage and the formation of the lesions.

In this study we did not directly measure phenolic content in the leaves, however, there is some, albeit weak, evidence for involvement of the peroxidase systems and possible oxidation of phenolics with increasing Mn exposure in *A. murale*. First, there are distinct changes in the 1,330–1,450 cm^{-1} spectral region of the

IR data (Fig. 9) with increasing Mn exposure. This region is indicative of O-H bending of alcohols and notably phenols and changes considerably in and after the Mn_{20} treatment where we saw the first signs of Mn toxicity. Second, we observed higher Ca concentrations within the lesion around the trichome in the SXRF maps (Fig. 6b). Calcium has been implicated in oxidative stress induced signaling and recently was shown to play a role in triggering peroxidase activity (Pleith and Vollbehr 2012). While not conclusive, these observations open the door to more research into the role that the peroxidase system and phenolics/phenoxy radicals play in lesion formation around trichomes on A. murale and other plants with similar patterns.

What does the loss of Mn lesions in Mn and Ni coexposed plants says about the mechanisms of Mn tolerance?

In plants co-exposed to Mn and Ni there were fewer necrotic lesions and Mn was preferentially sequestered in the basal compartment and rays of leaf trichomes (Fig. 5). The broadening in the 1,330–1,450 cm^{-1} region of the IR spectra in the $Mn_{50}Ni_{50}$ treated plants could possibly indicate the production of increased or different phenolics. Fecht-Christoffers et al. (2006) suggested that it may not only be the total quantity of phenols in the apoplast, but also the type which could have an influence on Mn tolerance. Perhaps, since the vacuole is the primary storage compartment of phenolics as well as Ni in *A. murale*, increased Ni concentrations influence the partitioning or production of phenolics in such a way that they are in greater supply or of a different type in the apoplastic space keeping it more reduced and leading to a more effective defense against oxidative damage.

We found via μ-XANES that some of the Mn in and around the trichomes of the Mn_{50} exposed plants was bound to citrate which is in agreement with other studies (Fernando et al. 2010). Horst et al. (1999) suggested that Mn bound to organic acids in the leaf apoplast may have contributed to the genotypic differences in Mn tolerance they observed in cow pea. It has also been shown that depending on what Mn is ligated to, it may act as an effective scavenger of ROS. Therefore the complexation of Mn with organic ligands together with their increased ROS scavenging potential may lead to greater or different capacities for Mn tolerance. Clearly additional analysis is necessary on a wider combination of Mn and Ni concentrations to tease out the influence that Ni additions are having on the distribution of Mn in and around trichomes, the speciation and partitioning of phenolics to the apoplastic space and the enzymes involved in this process.

Acknowledgments The authors would like to thank Dr. Jason Unrine for ICP-MS analysis of total metal concentrations, the environmental soil chemistry research group of Dr. Donald Sparks for the Mn standard spectra and Matthew Marcus at beamline 10.3.2 for advice on Mn fitting. The Advanced Light Source is supported by the Director, Office of Science, Office of Basic Energy Sciences, of the U.S. Department of Energy under Contract No. DE-AC02-05CH11231.

References

Ågren J, Schemske DW (1994) Evolution of trichome number in a naturalized population of Brassica rapa. American Naturalist 143:1–13

Beilstein MA, Al-Shehbaz IA, Kellogg EA (2006) Brassicaceae phylogeny and trichome evolution. American Journal of Botany 93(4):607–619

Beilstein MA, Al-Shehbaz IA, Mathews S, Kellogg EA (2008) Brassicaceae phylogeny inferred from phytochome A and NDHF sequence data: tribes and trichomes revisited. American Journal of Botany 95(10):1307–1327

Bani A, Pavlova D, Echevarria G, Mullaj A, Reeves RD, Morel JL, Sulce S (2010) Nickel hyperaccumulation by species of alyssum and Thlaspi (Brassicaceae) from the ultramafic soils of the Balkans. Botanica Servica 34(1):3–14

Barnese K, Gralla EB, Valentine JS, Cabelli DE (2012) Biologically relevant mechanisms for catalytic superoxide removal by simple manganese compounds. PNAS 109(18): 6892–6897

Benz BW, Martin CE (2006) Foliar trichomes, boundary layers, and gas exchange in the species of epiphytic Tillandsia (Bromeliaceae). J Plant Physiol 163:648–656

Blamey FPC, Joyce DC, Edwards DG, Asher CJ (1986) Role of trichomes in sunflower tolerance to manganese toxicity. Plant and Soil 91(2):171–180

Bray EA, Bailey SJ, Weretilnyk E (2000) Responses to abiotic stresses. In: Gruissem W, Buchannan B, Jones R (eds) Biochemistry and molecular biology of plants. American Society of Plant Biologists, Rockville, p 158

Broadhurst CL, Chaney RL, Angle JS, Erbe EF, Maugel TK (2004a) Nickel localization and response to increasing Ni soil levels in leaves of the Ni hyperaccumulator *Alyssum murale*. Plant and Soil 265(1–2):225–242

Broadhurst CL, Chaney RL, Angle JS, Maugel TK, Erbe EF, Murphy CA (2004b) Simultaneous hyperaccumulation of nickel, manganese, and calcium in Alyssum leaf trichomes. Environmental Science & Technology 38(21):5797–5802

Broadhurst LC, Tappero R, Maugel T, Erbe E, Sparks D, Chaney R (2009) Interaction of nickel and manganese in accumulation and localization in leaves of the Ni hyperaccumulators

Alyssum murale and *Alyssum corsicum*. Plant and Soil 314(1–2):35–48

Braodhurst LC, Bauchan GR, Murphy CA, Tang Y-T, Pooley C, Davis AP, Chaney RL (2013) Accumulation of zinc and cadmium and localization of zinc in Picris divaricata Vant. Environmental and Experimental Botany 87:1–9

Chaney RL (1988) Recent progress and needed research in plant Fe nutrition. Journal of Plant Nutrition 11(6–11):1589–1603

Ducic T, Thieme J, Polle A (2012) Phosphorus compartmentlazliation on the cellular level of Douglas Fir root as affected by Mn toxicity: a synchtrotron-based FTIR approach. Spectroscopy 27(5–6):265–272

Ducic T, Polle A (2007) Manangese toxicity in two varieties of Douglas fir (Pseudotsuga menziesii var. viridis and glauca) seedlings as afected by phosphours supply. Functional Plant Biology 34:31–40

Choi YE, Harada E, Kim GH, Yoon ES, Sano H (2004) Distribution of elements on tobacco trichomes and leaves under cadmium and sodium stresses. Journal of Plant Biology 47(2):75–82

Choi YE, Harada E, Wada M, Tsuboi H, Morita Y, Kusano T, Sano H (2001) Detoxification of cadmium in tobacco plants: formation and active excretion of crystals containing cadmium and calcium through trichomes. Planta 213(1):45–50

Choinski JS, Wise RR (1999) Leaf growth and development in relation to gas exchange in Quercus marilandica Muenchh. J Plant Physiol 154:302–309

De Silva DLR, Hetherington AM, Mansfield TA (1996) Where does all the calcium go? Evidence of an important regulatory role for trichomes in two calcicoles. Plant, Cell and Environment 19:880–886

Dou C, Fu X, Chen X, Shi J, Chen Y (2009) Accumulation and interaction of calcium and manganese in Phytolacca americana. Plant Science 177(6):601–606

Ehrlinger J (1984) Ecology and physiology of leaf pubescence in North American desert plants. In: Rodriguez E, Healey PL, Mehta I (eds) Biology and chemistry of plant trichomes. Plenum Press, New York, pp 113–132

El-Jaoual T, Cox DA (1998) Manganese toxicity in plants. Journal of Plant Nutrition 21(2):353–386

Fecht-Christoffers MM, Braun HP, Lemaitre-Guillier C, VanDorsselaer A, Horst WJ (2003) Effect of manganese toxicity on the proteome of the leaf apoplast in cowpea. Plant Physiology 133(4):1935–1946

Fecht-Christoffers MM, Fuhrs H, Braun HP, Horst WJ (2006) The role of hydrogen peroxide-producing and hydrogen peroxide-consuming peroxidases in the leaf apoplast of cowpea in manganese tolerance. Plant Physiology 140(4):1451–1463

Fecht-Christoffers MM, Horst WJ (2005) Does apoplastic ascorbic acid enhance manganese tolerance of Vigna unguiculata and Phaseolus vulgaris? Journal of Plant Nutrition and Soil Science-Zeitschrift Fur Pflanzenernahrung Und Bodenkunde 168(4):590–599

Fernando DR, Mizuno T, Woodrow IE, Baker AJM, Collins RN (2010) Characterization of foliar manganese (Mn) in Mn (hyper)accumulators using X-ray absorption spectroscopy. New Phytologist 188(4):1014–1027

Fernando DR, Mizuno T, Woodrow IE, Baker AJM, Marshall AT (2012) Plant homeostasis of foliar manganese sinks: Specific variation in hyperaccumulators. Planta 236(5):1459–1470

Foreman J, Demidchik V, Bothwell JHF, Mylona P, Miedema H, Torres MA, Linstead P, Costa S, Brownlee C, Jones JDG, Davies JM, Dolan L (2003) Reactive oxygen species produced by NADPH oxidase regulate plant cell growth. Nature 422(6930):442–446

Freeman JL, Lindblom SD, Quinn CF, Fakra S, Marcus MA, Pilon-Smits EAH (2007) Selenium accumulation protects plants from herbivory by orthoptera due to toxicity and deterrence. New Phytologist 175:490–500

Galvez L, Clark RB, Gourley LM, Maranville JW (1989) Effects of silicon on mineral-composition of sorghum grown with excess manganese. Journal of Plant Nutrition 12(5):547–561

Ghasemi R, Ghaderian SM, Kramer U (2009) Accumulation of nickel in trichomes of a nickel hyperaccumulator plant, Alyssum inflatum. Northeastern Naturalist 16:81–92

Hansard SP, Easter HD, Voelker BM (2011) Rapid reaction of nanomolar Mn(II) with superoxide radical in seawater and simulated freshwater. Environmental Science & Technology 45(7):2811–2817

Hansel CM, Zeiner CA, Santelli CM, Webb SM (2012) Mn (II) oxidation by an ascomycete fungus is linked to superoxide production during asexual reproduction. Proc Natl Acad Sci 109:12621–12625

Harada E, Choi YE (2008) Investigation of metal exudates from tobacco glandular trichomes under heavy metal stresses using a variable pressure scanning electron microscopy system. Plant Biotechnology 25(4):407–411

Herndon EM, Jin LX, Brantley SL (2011) Soils reveal widespread manganese enrichment from industrial inputs. Environmental Science & Technology 45(1):241–247

Horiguchi T (1987) Mechanism of manganese toxicity and tolerance of plants 2. deposition of oxidized manganese in plant-tissues. Soil Science and Plant Nutrition 33(4):595–606

Horst WJ (1988) The physiology of manganese toxicity. In: Graham RD, Hannam RJ, Uren NJ (eds) Manganese in soil and plants. Kluwer Academic Publishers, Dordrecht, pp 175–188

Horst W, Fecht M, Naumann A, Wissemeier A, Maier P (1999) Physiology of manganese toxicity and tolerance in Vigna unguiculata (L.) Walp. J Plant Nutr Soil Sci 162:263–274

Isaure M, Fayard B, Sarret G, Pairis S, Bourguignon J (2006) Localization and chemical forms of cadmium in plant samples by combining analytical electron microscopy and X-ray spectromicroscopy. Spectrochimica Acta Part B 61:1242–1252

Isaure MP, Sarret G, Harada E, Choi YE, Marcus MA, Fakra SC, Geoffroy N, Pairis S, Susini J, Clemens S, Manceau A (2010) Calcium promotes cadmium elimination as vaterite grains by tobacco trichomes. Geochimica Et Cosmochimica Acta 74(20):5817–5834

Jeffree CE (1986) The cuticle, epicuticular waxes and trichomes of plants, with reference to their structure, function and evolution. In: Juniper B, Southwood SR (eds) Insects and the plant surface. Arnold, London, pp 23–64

Kamiya T, Akahori T, Maeshima M (2005) Expression profile of the genes for rice cation/H+exchanger family and functional analysis in yeast. Plant and Cell Physiology 46(10):1735–1740

Kamiya T, Akahori T, Maeshima M (2006) Expression profile of the genes for rice cation/H+exchanger family and functional analysis in yeast. Plant and Cell Physiology 47:S201–S201

Karban R, Baldwin IT (1997) Induced responses to herbivory. The University of Chicago Press, Chicago, p 319

Kramer U, Grime GW, Smith JAC, Hawes CR, Baker AJM (1997) Micro-PIXE as a technique for studying nickel localization in leaves of the hyperaccumulator plant Alyssum lesbiacum. Nuclear Instruments & Methods in Physics Research Section B-Beam Interactions with Materials and Atoms 130(1–4):346–350

Kukier U, Peters CA, Chaney RL, Angle JS, Roseberg RJ (2004) The effect of pH on metal accumulation in two Alyssum species. Journal of Environmental Quality 33(6):2090–2102

Küpper H, Lombi E, Zhao FJ, McGrath SP (2000) Cellular compartmentation of cadmium and zinc in relation to other elements in the hyperaccumulator Arabidopsis halleri. Planta 212(1):75–84

Küpper H, Lombi E, Zhao FJ, Wieshammer G, McGrath SP (2001) Cellular compartmentation of nickel in the hyperaccumulators Alyssum lesbiacum, Alyssum bertolonii and Thlaspi goesingense. Journal of Experimental Botany 52(365):2291–2300

Levin DA (1973) The role of trichomes in plant defence. Quarterly Review of Biology 48:3–15

Macnicol RD, Beckett PHT (1985) Critical tissue concentrations of potentially toxic elements. Plant and Soil 85:107–129

Marschner P (2012) Marschner's mineral nutrition of higher plants. Elsevier, London

Marcus MA, MacDowell AA, Celestre R, Manceau A, Millter T, Pdmore HA, Sublett RE (2004) Beamline 10.3.2 at ALS: A hard X-ray microprobe for environemtnal and materials sciences. J Synchrotron Radiat 1(11):239–247

McNear DH, Peltier E, Everhart J, Chaney RL, Sutton S, Newville M, Rivers M, Sparks DL (2005) Application of quantitative fluorescence and absorption-edge computed microtomography to image metal compartmentalization in *Alyssum murale*. Environmental Science & Technology 39(7):2210–2218

Pittman JK (2005) Managing the manganese: Molecular mechanisms of manganese transport and homeostasis. New Phytologist 167(3):733–742

Pittman JK, Shigaki T, Marshall JL, Morris JL, Cheng NH, Hirschi KD (2004) Functional and regulatory analysis of the Arabidopsis thaliana CAX2 cation transporter. Plant Molecular Biology 56(6):959–971

Pittman JK, Shigaki T, Morris JL, Hirschi KD (2005) Functional analysis of CAX2, an Arabidopsis cation/proton transporter with broad specificity. Comparative Biochemistry and Physiology a-Molecular & Integrative Physiology 141(3): S272–S272

Pleith C, Vollbehr S (2012) Calcium promotes actiivty and confers heat stability on plant peroxidases. Plant Signal Bahav 7(6): On-line first.

Psaras GK, Constantinidis T, Cotsopoulos B, Manetas Y (2000) Relative abundance of nickel in the leaf epidermis of eight hyperaccumulators: Evidence that the metal is excluded from both guard cells and trichomes. Annals of Botany 86(1):73–78

Quinn CF, Prins CN, Gross AM, Hantzis L, Reynolds RJB, Freeman JL, Yang SI, Covey PA, Bañuelos GS, Pickering IJ, Fakra SF, Marcus MA, Arathi HS, Pilon-Smits EAH (2011) Selenium accumulation in flowers and its effects on pollination. New Phytologist 192:727–737

Reeves RD, Baker AJ (2000) Metal-accumulating plants. In: Raskin I, Ensley BD (eds) Phytoremediation of toxic metals: Using plants to clean up the environment. Wiley, New York, pp 193–229

Sakihama Y, Cohen MF, Grace SC, Yamasaki H (2002) Plant phenolic antioxidant and prooxidant activities: phenolics-induced oxidative damage mediated by metals in plants. Toxicology 177(1):67–80

Sarret G, Harada E, Choi YE, Isaure MP, Geoffroy N, Fakra S, Marcus MA, Birschwilks M, Clemens S, Manceau A (2006) Trichomes of tobacco excrete zinc as zinc-substituted calcium carbonate and other zinc-containing compounds. Plant Physiology 141(3):1021–1034

Sarret G, Isaure MP, Marcus MA, Harada E, Choi YE, Pairis S, Fakra S, Manceau A (2007) Chemical forms of calcium in Ca, Zn- and Ca, Cd-containing grains excreted by tobacco trichomes. Canadian Journal of Chemistry-Revue Canadienne De Chimie 85(10):738–746

Sarret G, Saumitou-Laprade P, Bert V, Proux O, Hazemann JL, Traverse AS, Marcus MA, Manceau A (2002) Forms of zinc accumulated in the hyperaccumulator Arabidopsis halleri. Plant Physiology 130(4):1815–1826

Sarret G, Willems G, Isaure MP, Marcus MA, Fakra SC, Frerot H, Pairis S, Geoffroy N, Manceau A, Saumitou-Laprade P (2009) Zinc distribution and speciation in Arabidopsis halleri x Arabidopsis lyrata progenies presenting various zinc accumulation capacities. New Phytologist 184(3):581–595

Schaaf G, Catoni E, Fitz M, Schwacke R, Schneider A, von Wiren N, Frommer WB (2002) A putative role for the vacuolar calcium/manganese proton antiporter AtCAX2 in heavy metal detoxification. Plant Biology 4(5):612–618

Southwood SR (1986) Plant surfaces and insects—an overview. In: Juniper B, Southwood SR (eds) Insects and the plant surface. Arnold, London, pp 1–22

Tappero RV (2008) Microspectroscopic study of cobalt speciation and localization in nickel hyperaccumulator *Alyssum murale*. Ph.D. Dissertation, University of Delaware, Newark

Traw BM, Dawson TE (2002) Reduced performance of two specialist herbivores (Lepidoptera: Pieridae, Coleoptera: Chrysomelidae) on new leaves of damaged black mustard plants. Environmental Entomology 31:714–722

Tumi AF, Mihailović N, Gajić BA, Niketić M, Tomović G (2012) Comparative study of hyperaccumulation of nickel by *Alyssum murale* s.l. populations from the ultramafics of Serbia. Pol J Environ Stud 21(6):1855–1866

Wagner G, Wang E, Shepherd RW (2004) New approaches for studying and exploiting an old protuberance, the plant trichome. Annals of Botany 93:3–11

Webb MA (2007) Calcium biominerals in trichomes of the Brassicaceae. Plant Biology Meetings. July 7–12 Chicago, Illinois

Werker E (2000) Trichome diversity and development. Advances in Botanical Research Incorporating Advances in Plant Pathology 31:1–35

Wissemeier AH, Horst WJ (1992) Effect of light-intensity on manganese toxicity symptoms and callose formation in cowpea (Vigna-Unguiculata (L) Walp). Plant and Soil 143(2):299–309